

RSC Advances



This is an *Accepted Manuscript*, which has been through the Royal Society of Chemistry peer review process and has been accepted for publication.

Accepted Manuscripts are published online shortly after acceptance, before technical editing, formatting and proof reading. Using this free service, authors can make their results available to the community, in citable form, before we publish the edited article. This *Accepted Manuscript* will be replaced by the edited, formatted and paginated article as soon as this is available.

You can find more information about *Accepted Manuscripts* in the [Information for Authors](#).

Please note that technical editing may introduce minor changes to the text and/or graphics, which may alter content. The journal's standard [Terms & Conditions](#) and the [Ethical guidelines](#) still apply. In no event shall the Royal Society of Chemistry be held responsible for any errors or omissions in this *Accepted Manuscript* or any consequences arising from the use of any information it contains.

ARTICLE

Synthesis of γ -Fe₂O₃/TiO₂ nanocomposite and its application to the removal of dyes from water samples by adsorption and degradation processes

Cite this: DOI: 10.1039/x0xx00000x

Received 00th January 2012,

Accepted 00th January 2012

DOI: 10.1039/x0xx00000x

www.rsc.org/

Tayyebeh Madrakian*, Abbas Afkhami, Reza Haryani and Mazaher Ahmadi

New facile route have been proposed for the synthesis of γ -Fe₂O₃/TiO₂ nanocomposite. The synthesized nanocomposite was fully characterized by TEM, VSM, EDX and XRD measurements. Dye removal ability of the synthesized nanoparticles was investigated by the evaluation of its removal efficiency in the removing of Janus Green B, as a cationic dye, and Congo red, as an anionic dye. Dye degradation ability of the synthesized nanocomposite was investigated under the various irradiation lights (i.e. sunlight, 254 nm and 365 nm UV light). The results showed that the new route result in new TiO₂ nanocomposite with improved photocatalytic activity under sunlight irradiation. Also, the results showed that the synthesized nanocomposite could be considered as an efficient photocatalyst in the field of wastewater treatment due to its lower band gap in the presence of γ -Fe₂O₃ nanoparticles.

Introduction

Photocatalytic activity has been receiving a great attention research area for several years in the case of its application in water concomitant degradation and wastewater treatment. TiO₂ is one of the most commonly used photocatalysts in this field¹⁻⁶, because of its strong oxidizing abilities for the decomposition of organic pollutants, super hydrophilicity, chemical stability, long durability, nontoxicity, low cost, and transparency to visible light⁷. However, because of its high band gap energy, its application is limited to excitation in the ultra-violet region. Therefore it requires a UV source for band gap excitation during photocatalysis. The photocatalytic properties of TiO₂ are due to the formation of photogenerated hole and electron charge carriers, which occurs upon the absorption of ultraviolet light corresponding to the band gap. The photogenerated holes in the valence band diffuse to the TiO₂ surface and react with the adsorbed water molecules, forming hydroxyl radicals. The photogenerated holes and the hydroxyl radicals oxidize nearby organic molecules on the TiO₂ surface. Meanwhile, electrons in the conduction band stereotypically participate in the reduction processes, which typically react with molecular oxygen in the air to produce superoxide radical anions⁷. Only 5% of the UV light from the solar beam reaches the earth. Hence TiO₂ is rarely excited by the solar beam that reaches the earth.^{8,9} One of the potential solutions for improving the photocatalytic efficiency of TiO₂ in the visible region is to shift its optical absorption from the UV region to the visible-light region,

allowing for more photons to be absorbed and utilized in decomposing the pollutants¹⁰. It has been widely recognized that the efficiency of photocatalytic reactions of TiO₂ materials can be enhanced *via* deposition of transition metals¹¹⁻¹⁴, doping with non-metals¹⁵⁻¹⁷, coupling TiO₂ with narrow band-gap semiconductors^{18,19} and preparing oxygen-deficient TiO₂^{20,21}.

Metal oxide core-shell nanocomposites offer a potential solution as a result of the synergy that is possible among the components¹⁰. TiO₂ based photocatalytic hetero structures such as noble metal/TiO₂²² carbon/TiO₂²³ metal oxide/TiO₂²⁴ and metal chalcogenide/TiO₂²⁵ have been proposed and studied. γ -Fe₂O₃, one of the stable forms of iron oxide under ambient conditions, is a promising material for the catalysis and gas sensors²⁴⁻²⁶, which is in addition to its widely application in pollutant adsorption removal²⁷⁻³¹, due to of its stability, magnetic properties, lower band gap, easy synthesis and low cost. The combination of TiO₂ with Fe₂O₃ can decrease the recombination rate of photogenerated electrons and holes in resultant nanocomposite. Furthermore, the core-shell structured Fe₂O₃/TiO₂ nanocomposites can be used to improve the visible light response of TiO₂.^{10, 32-34}

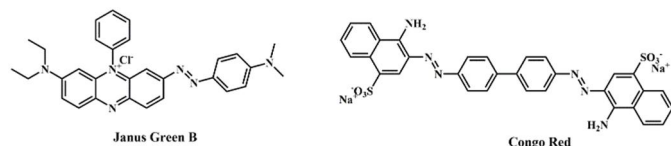
This work reports on a new route for the synthesis of γ -Fe₂O₃/TiO₂ nanocomposite. Catalytic properties of the synthesized nanocomposite show an improvement in catalytic activity under sunlight irradiation condition as compared with bare TiO₂ nanoparticles. The synthesized nanocomposite was applied to the removing of Janus Green B (JG) and Congo Red (CR) from water samples. Contribution of the adsorption and

photodegradation processes in the removal of JG and CR dyes was evaluated by chemical oxygen demand (COD) tests. The results showed that the synthesized nanocomposite could be considered as an efficient photocatalyst in the field of wastewater treatment due to its lower band gap in the presence of γ -Fe₂O₃ nanoparticles as compared with TiO₂ nanoparticles.

Experimental

Reagents and materials

All the chemicals used were of analytical reagent grade or the highest purity available and were purchased from Merck Company (Darmstadt, Germany). Double distilled water (DDW) was used throughout the work. TiO₂ nanoparticles (Titanium (IV) oxide, anatase nanopowder, <25 nm particle size) was purchased from Aldrich. All glassware were soaked in dilute nitric acid for 12 h and then thoroughly rinsed with DDW. The dyes stock solutions were prepared in DDW and working standard solutions of different dye concentrations were prepared daily by diluting the stock solution with DDW. The adjustment of pH was performed with 0.01-1.0 mol L⁻¹ HCl and/or NaOH solutions. Scheme 1 shows the structure of the investigated dyes.



Scheme 1 The structure of the investigated dyes.

Apparatus

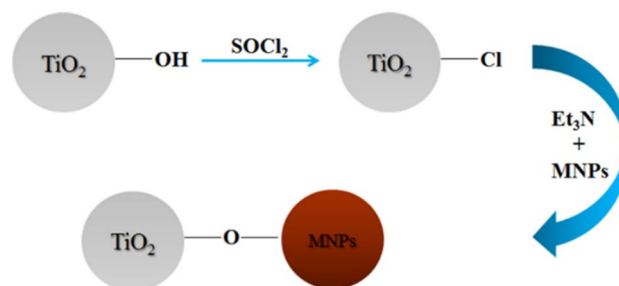
The size, morphology and structure of the nanoparticles were characterized by transmission electron microscopy (TEM, Philips-CMC-300 KV). The crystal structure of the synthesized nanoparticles was determined by an X-ray diffractometer (XRD, 38066 Riva, d/G. via M. Misone, 11/D (TN) Italy) at ambient temperature. The chemical composition of the prepared nanoparticles was measured by EDX performed in a scanning electron microscope (VEGA TEScan SEM). The magnetic properties of the nanoparticles were measured with a vibrating sample magnetometer (VSM, 4 in. Daghigh Meghnatis Kashan Co., Kashan, Iran).

A Metrohm model 713 pH-meter was used for pH measurements. A single beam UV-mini-WPA spectrophotometer was used for the determination of the dyes concentration in the solutions. A 40 kHz universal ultrasonic cleaner water bath (RoHS, Korea) was used.

Preparation of γ -Fe₂O₃ nanoparticles (MNPs) and γ -Fe₂O₃/TiO₂ nanocomposite (MNPTiO₂)

MNPs were prepared according to the previously reported procedure²⁷. MNPTiO₂ was synthesized according to the following procedure (scheme 2): typically 7.0 mL of thionyl chloride and 0.5 g of TiO₂ nanoparticles were brought into a

25.0 mL flask and refluxed for 12.0 h at 90°C. After completion of the reaction, unreacted thionyl chloride was distilled at 100 °C, and then 20.0 mL triethyl amine and 1.0 g MNPs were added to the produced nanoparticles. Then the mixture was refluxed overnight at 45°C. The resultant γ -Fe₂O₃/TiO₂ nanocomposite was washed using methanol and DDW and dried under the vacuum at 80°C.



Scheme 2 Schematic diagram for synthesis of γ -Fe₂O₃/TiO₂ nanocomposite.

Dye removal experiment

Adsorption studies were performed by adding 0.02 g of MNPTiO₂ to 25.0 mL solution of different concentrations of dyes in a 50 mL beaker. The solution was stirred for 25.0 min. Then the dye loaded MNPTiO₂ was separated with magnetic decantation. The concentration of dye in the solution was measured spectrophotometrically at the wavelength of the maximum absorbance of each dye (λ_{\max} (JG): 612 nm, λ_{\max} (CR): 492 nm). The concentration of dyes decreased with time due to their adsorption and, to some extent, degradation by fMNPTiO₂. The adsorption percent for each dye, i.e. the dye removal efficiency, was determined using the following expression:

$$\% \text{ Re} = \left[\frac{(C_0 - C_e)}{C_0} \right] \times 100 \quad (1)$$

where C_0 and C_e represent the initial and equilibrium (after adsorption) concentrations of each dye in mg L⁻¹, respectively. Dye uptake, q_e (mg dye per g MNPTiO₂), was determined by mass balance, as follows:

$$q_e = (C_0 - C_e) \times \frac{V}{m} \quad (2)$$

where V is the volume of the solution in L, and m is the mass of MNPTiO₂ (g).

Photodegradation reactions and COD tests

The photocatalytic activities of the investigated nanoparticles were evaluated by the degradation of JG and CR dyes in an aqueous solution under the irradiation of both ultraviolet (UV) light (at 254 nm and/or 365 nm) and sunlight. The reactions were conducted at ambient temperature and pressure. The 36 W Hg lamp (254 nm, TUV 36W/G36TB, Philips, Holland) and 36 W Xe lamp (365 nm, LT 36W/009W, HRA 4348, Germany) were used as the UV light sources, to trigger the photocatalytic reactions, at 10 cm distance from reaction vessel. Typically, the aqueous dye-MNPTiO₂

suspension system was prepared as follows. A 10.0 g sample of the MNPTiO_2 was dispersed in a 50 mL aqueous solution containing various concentrations of each dye ($C_0 = 5.0, 20.0, 30.0, 50.0, 100.0, 200.0, 400.0 \text{ mg L}^{-1}$). The mixture was stirred for 10 min in the dark to achieve the adsorption–desorption equilibrium before the irradiation. The suspension was stirred before and during the illumination. After completion of the procedure, the residual concentration of each dye was detected spectrophotometrically at the wavelength of the maximum absorbance of each dye. In order to distinguish participation of adsorption from degradation (under sunlight illumination), COD test was performed on residual solution. COD test was performed according to “Macro COD by reflux digestion and titration” method³⁵ using standard potassium dichromate solution as an oxidizing agent.

Adsorption isotherms

The equilibrium data were analyzed in accordance with the Langmuir and Freundlich isotherm models.

The linear form of the Langmuir isotherm is³⁶:

$$\frac{C_e}{q_e} = \frac{1}{K_L q_m} + \frac{1}{q_m} C_e \quad (3)$$

where K_L is a constant and q_m is the maximum amount of the solute adsorbed per gram of the sorbent (mg g^{-1}), which depends on the number of adsorption sites. The Langmuir isotherm shows that the amount of dye adsorption increases as the concentration increases up to a saturation point.

The linear form of Freundlich empirical model is represented by³⁷:

$$\ln q_e = \ln k_f + \frac{1}{n} \ln C_e \quad (4)$$

where K_f ($\text{mg}^{1-1/n} \text{ L}^{1/n} \text{ g}^{-1}$) and $1/n$ are Freundlich constants depending on the temperature and the given adsorbent–adsorbate couple. The parameter n is related to the adsorption energy distribution, and K_f indicates the adsorption capacity.

Results and Discussion

Characterization of the investigated nanoparticles

The morphology and crystallographic structure of the investigated nanoparticles were characterized using transmission electron microscopy (TEM) and X-ray diffraction (XRD). The TEM image in Fig. 1a shows that the average diameter of the synthesized MNPs is around 20 nm. TEM image of MNPTiO_2 (Fig. 1b) shows morphological properties of the MNPTiO_2 nanocomposite. From this Fig. it can be concluded that the nanoparticle aggregation and attachments have been occurred. The XRD pattern of the synthesized products is shown in Fig. 2. As Fig 2 shows, all the peaks of MNPs (Fig. 2a) and TiO_2 nanoparticles (Fig. 2b) can be seen in the MNPTiO_2 spectrum (Fig. 2c). This indicates that MNPTiO_2 nanocomposite has been synthesized.

A quantitative EDX spectrum was taken to determine the elemental composition of the MNPTiO_2 nanocomposite. The results are presented in Fig. 3. The EDX spectrum confirmed

that there were no elemental impurities present in the nanocomposite composition. The analysis of the spectrum was also performed to find the weight percent (Wt %) and atomic percent (At %) of each element, which is given in Table 1.

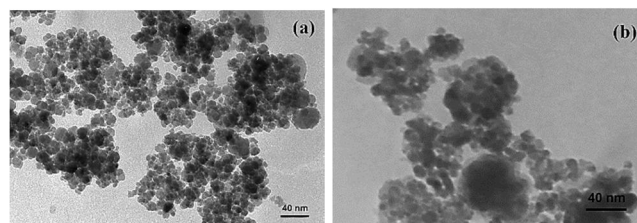


Fig. 1 TEM image of (a) MNPs and (b) MNPTiO_2 nanoparticles.

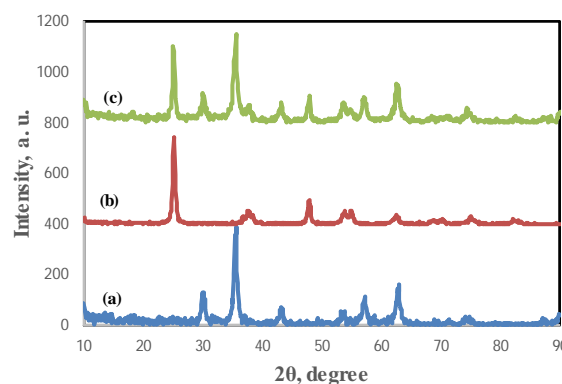


Fig. 2 XRD pattern of (a) MNPs, (b) TiO_2 and (c) MNPTiO_2 nanoparticles.

Table 1 EDX elemental composition of the MNPTiO_2 nanocomposite.

Element	Wt%		At%	
	Experimental	Theoretical	Experimental	Theoretical
Oxygen	30.10	33.33	60.52	62.43
Titanium	27.87	20.00	18.72	12.52
Iron	36.03	46.67	20.75	25.05

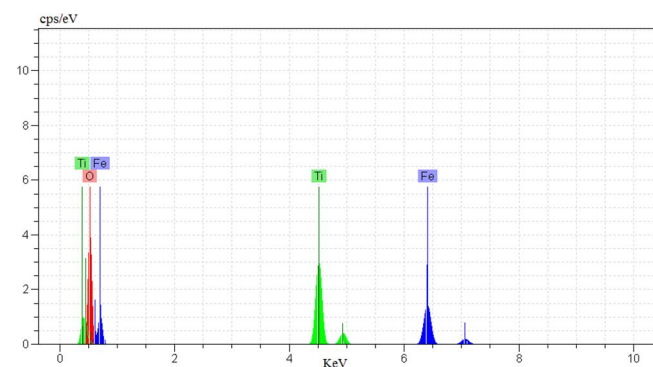


Fig. 3 EDX spectrum of the MNPTiO_2 nanocomposite.

The magnetization curves of the MNPs and MNPTiO_2 nanocomposite, recorded with a VSM, are illustrated in Fig. 4. As shown in Fig. 4, the magnetization of the samples would approach the saturation values when the applied magnetic field increases to 10,000 Oe. The saturation magnetization of the MNPs nanoparticles was obtained as 60.85 emu/g. For

MNPTiO₂ nanocomposite, the saturation magnetization was found to be 54.66 emu/g. These results show that magnetic properties are affected by the surface modification. A magnetization reduction of about 10% was observed between uncoated and TiO₂-coated MNPs. This may be related to the nanoparticle size effect, the increased surface disorder, and the diamagnetic contributions of TiO₂ nanoparticles. The amount of decrease was not too large to seriously affect the use of these nanoparticles for the desired application.

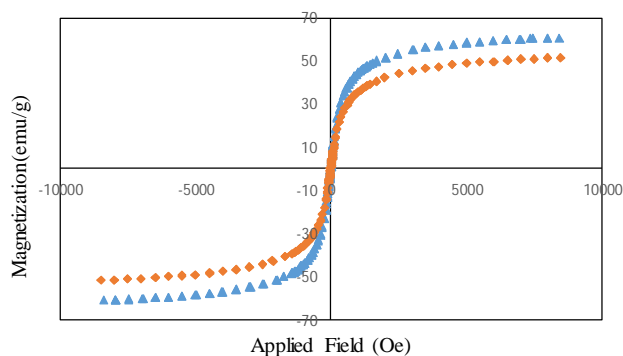


Fig. 4 Magnetization curves obtained by vibrating sample magnetometer (VSM) at room temperature: (▲) MNPs nanoparticles and (◆) MNPTiO₂ nanocomposite.

Effect of solution initial pH on dye uptake

Solution pH affects adsorption process of dye molecules by affecting both aqueous chemistry and surface binding-sites of the adsorbent. The effect of pH in the range 3.0–12.0 with a stirring time of 45 min on the removing of dyes was investigated using 0.1 mol L⁻¹ HCl and/or NaOH solutions for pH adjustment. The initial dye concentration was fixed at 50.0 mg L⁻¹. Fig. 5 shows the removal efficiency variations as a function of pH for each dye. As Fig. 5 shows, the removal percentage in the case of JG increased by increasing pH, reached a maximum at pH 11.0 and remained nearly constant at higher pHs. For CR, the maximum removal occurred at pH 4.0. Therefore, pH 11.0 was selected for JG and pH 4.0 was chosen for CR.

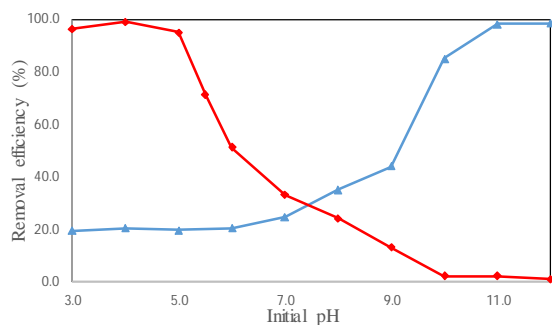


Fig. 5 Removal efficiency percentage at different pHs for JG (▲) and CR (◆). Conditions: 0.01g of MNPTiO₂, 25.0 mL of 50.0 mg L⁻¹ of dye, agitation time of 45 min.

The point of zero charge, pH_{pzc}, of MNPTiO₂ in aqueous solution was found to be 6.2 and negative zeta potential increased with increasing alkaline solution pH. In other words, the predominant charge at the MNPTiO₂ in acidic solutions is positive. Therefore, for the anionic dye CR, high efficiency removal was obtained at low pHs. It seems that the dominant mechanism of the adsorption is electrostatic attraction³⁸. At pH 4 and below it, a considerable high electrostatic attraction exists between the positively charged surface of the adsorbent and negatively charged anionic dye molecules. By increasing the pH of the solution, the adsorption of the anionic dye at MNPTiO₂ tends to decrease, which can be explained by the increasing electrostatic repulsion between the anionic dye adsorbate species and negatively charged adsorbent surfaces. Also lower adsorption at alkaline pHs can be due to the presence of OH⁻ ions that causes destabilizing anionic dye and competing with the dye anions for the adsorption sites. In the case of the cationic dye a similar behavior, but in the opposite direction, was observed.

Effect of adsorbent dosage on dye removal

The dependence of the adsorption of dye on the amount of MNPTiO₂ was studied at room temperature and at optimum pH for each dye by varying the adsorbent amount from 0.01–0.04 g in contact with 25.0 mL solution of 50.0 mg L⁻¹ of each dye. The percentage removal of dye increased by increasing the amount of MNPTiO₂, apparently due to the availability of the higher adsorption sites. The adsorption reached a maximum with 0.02 g of adsorbent for both dyes. The maximum percentage removal was about 98%.

Effect of contact time

The effect of contact time on the adsorption of the investigated dyes was studied to determine the time taken by MNPTiO₂ to remove 50.0 mg L⁻¹ dye solution at the optimum pH. An optimum value of MNPTiO₂ was added into a 25.0 mL of the dye solution. Absorbance of the solution at λ_{max} with time was determined to monitor the dye concentration. It was observed that almost all of the both dyes became adsorbed after 25.0 min. Therefore, agitation time of 25.0 min was selected for further works.

Photocatalytic Activity

The dye removal process took place by both the adsorption and photocatalytic processes at the sorbent. In order to estimate the contribution of each process, the amount of the dye became adsorbed was determined after desorption by eluent. Solutions of 50.0 mg L⁻¹ of JG and CR were added to 20 mg of nanoparticles. After 25.0 min the total removal of the dyes were determined and then the nanoparticles were separated and the amount of the adsorbed dyes were determined after desorption. The results indicated a contribution of 15.0 and 19.0 % dye removal by photocatalytic effect for JG and CR, respectively. The photodegradation efficiency increased by increasing of the time. The photodegradation contribution of the dyes removal increased to 22.0 and 30.0 % for JG and CR after 60.0 min,

respectively. The results also indicated the photodegradation efficiency for CR is higher than that for JG, this may be related to the effect of structure of the dye. In conclusion, these results confirm that the TiO₂ shell in the MNPs is photocatalytically active and promotes the dyes removal. Also the results reveal that the magnetic core interact on removal of dyes.

Adsorption isotherms

The capacity of the adsorbent is an important factor that determines how much sorbent is required for quantitative removal of a specific amount of the dyes from solution. For measuring the adsorption capacity of MNPTiO₂, the adsorbent was added into the JG and CR solutions at various concentrations, and the suspensions were stirred at room temperature and under sunlight, followed by magnetic removal of the adsorbent. An adsorption isotherm describes the fraction of the sorbate molecules that are partitioned between the liquid and the solid phase at equilibrium. Adsorption of the dyes by the adsorbent was modeled using Freundlich and Langmuir adsorption isotherms. After subtraction of photodegradation contribution, the remained dyes in the supernatants were

measured spectrometrically at corresponding maximum absorption wavelength of each dye, and the results were used to plot the isothermal adsorption curves as shown in Fig. 6. The equilibrium adsorption data were fitted to Langmuir and Freundlich isotherm models by linear regression. The resulting parameters are summarized in Tables 2 and 3.

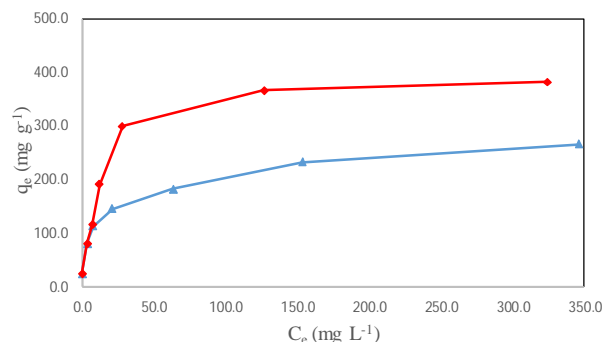


Fig. 6 Isothermal adsorption curves of CR (♦) and JG (▲) on MNPTiO₂ adsorbents.

Table 2 Adsorption isotherm parameters for Langmuir and Freundlich adsorption isotherms in the case of JG removal.

Isotherm models Parameters	Langmuir			Freundlich		
	K _L (L mg ⁻¹)	q _m (mg g ⁻¹)	R ²	K _F	1/n	R ²
MNPs (sunlight)	0.17	140.84	0.9989	46.99	0.22	0.8633
TiO ₂ (sunlight)	0.21	131.57	0.9994	42.94	0.22	0.6857
TiO ₂ (254 nm)	0.28	294.11	0.9987	131.63	0.15	0.8533
TiO ₂ (365 nm)	0.036	175.43	0.9975	19.68	0.39	0.8597
MNPTiO ₂ (sunlight)	0.068	270.27	0.9933	47.94	0.32	0.9653
MNPTiO ₂ (254 nm)	0.10	285.71	0.9973	55.70	0.32	0.9132
MNPTiO ₂ (365 nm)	0.10	277.77	0.9964	79.04	0.22	0.9275

Table 3 Adsorption isotherm parameters for Langmuir and Freundlich adsorption isotherms in the case of CR removal.

Isotherm models Parameters	Langmuir			Freundlich		
	K _L (L mg ⁻¹)	q _m (mg g ⁻¹)	R ²	K _F	1/n	R ²
MNPs (sunlight)	0.08	357.14	0.9976	54.59	0.36	0.9257
TiO ₂ (sunlight)	0.06	285.17	0.9961	39.25	0.37	0.9177
TiO ₂ (254 nm)	0.35	416.66	0.9997	137.01	0.21	0.9113
TiO ₂ (365 nm)	0.13	322.25	0.9968	86.48	0.24	0.9558
MNPTiO ₂ (sunlight)	0.09	400.10	0.9981	50.90	0.41	0.8999
MNPTiO ₂ (254 nm)	0.10	434.87	0.9985	66.02	0.38	0.9003
MNPTiO ₂ (365 nm)	0.18	400.21	0.9991	113.29	0.26	0.6889

The correlation coefficient obtained for the Langmuir model ($R^2 > 0.99$) indicates that the experimental data are better fitted into this model, and adsorption of the investigated dyes on MNPTiO₂ is more compatible with Langmuir assumptions, i.e., adsorption takes place at specific homogeneous sites within the adsorbent. The Langmuir model is based on the physical hypothesis that the maximum adsorption capacity consists of a monolayer adsorption, that there are no interactions between adsorbed molecules, and that the adsorption energy is distributed homogeneously over the entire coverage surface. This sorption model serves to estimate the maximum uptake values where they cannot be reached in the experiments.

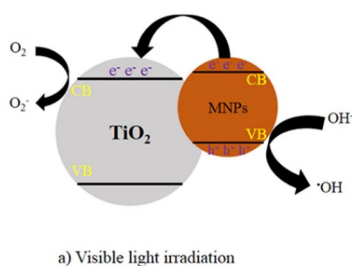
In order to investigate the surface modification and various irradiation condition effects on the dye removal ability of the

adsorbent, isothermal studies was conducted by three types of adsorbents (i.e. MNPs, TiO₂ and MNPTiO₂) under various irradiation conditions (sunlight, 254 nm and 365 nm). The results are summarized in Tables 2 and 3.

According to the results of EDX analysis (Table 1) the percentage of TiO₂ nanoparticles/MNPs is almost 50%. So if it is supposed that MNPTiO₂ nanocomposite will be a simple mixture of TiO₂ nanoparticles and MNPs, based on the result of Tables 2 and 3, the removal ability of the nanocomposite under sunlight irradiation condition shows a clear improvement.

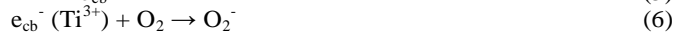
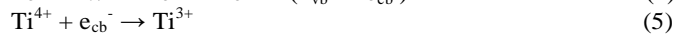
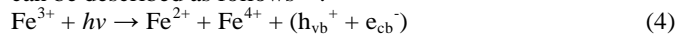
MNPTiO₂ nanocomposites exhibited a poor photocatalytic activity under UV irradiation in comparison with sunlight irradiation. The activity of photocatalytic degradation reaction depends on many factors, such as the adsorption of dye at the

catalyst surface, band-gap energy, surface area, particle size, crystallinity, and electron-hole recombination rate¹⁰. For the recently synthesized MNPTiO₂ nanocomposite, the photocatalytic activity under visible and UV light irradiation is mainly dependent on band-gap structure and the relationship between the fast recombination rate of charge carriers in comparison with the reactions decomposing the dyes. Generally, when MNPs were coupled to the surface of TiO₂, the Fermi level of TiO₂ and MNPs must align in equilibrium due to the presence of the MNPs/TiO₂ heterojunction. Under the visible light irradiation, TiO₂ cannot be excited to generate electron-hole pairs, whereas MNPs could be easily activated and yield charge carriers, as shown in scheme 3a¹⁰.



Scheme 3 Suggested electronic transition between TiO₂ and MNPs under sunlight and UV light irradiation.

Subsequently, the photogenerated electrons immigrate from the conduction band of MNPs to the conduction band of TiO₂ under the action of built-in electric field and the concentration gradient activated and yielded charge carriers, while photogenerated holes accumulated in the valence band of MNPs^{10, 39, 40}. The negative electrons in the valence band of TiO₂ will further react with molecular oxygen dissolved in the dye solution to form the superoxide anion and hydrogen peroxide. While the accumulated holes in the valence band of MNPs will react with OH species existing on the surface of the catalyst to produce reactive hydroxyl radicals. The reactions can be described as follows¹⁰:



However, under the irradiation of UV light, electron-hole pairs are produced in the conduction and valence bands of TiO₂, a heterojunction is formed between MNPs and TiO₂ becomes normal^{41, 42}, the MNPs would act as recombination centers of the photogenerated electrons and holes, as illustrated in scheme 3b. MNPs will absorb most of the electromagnetic irradiation and promote favorable conditions for the presence of hole-electron recombination centers, so that MNPTiO₂ nanocomposites exhibit a poor photocatalytic activity under UV irradiation in comparison with sunlight irradiation.

Table 4 The COD results under sunlight irradiation condition.

Catalyst	Compound	Initial COD (mg L ⁻¹)	Final COD (mg L ⁻¹)
MNPTiO ₂	CR	101.5	92.3

	JG	139.0	125.1
TiO ₂	CR	101.5	99.4
	JG	139.0	136.4

In order to evaluate the adsorption portion from degradation part, in removal of the JG and CR dyes, COD tests was performed. The results are summarized in Table 4.

As can be seen, COD decrement in the case of the synthesized nanocomposite is somewhat higher than that of TiO₂ nanoparticles, suggesting that there is an improvement in photocatalytic activity of the synthesized nanocomposite.

Conclusions

In summary, the γ -Fe₂O₃/TiO₂ nanocomposite has been fabricated via a new facile route. Photocatalytic degradation of JG, as a cationic dye, and CR, as an anionic dye, in the liquid phase was used to evaluate the activity of the synthesized nanocomposites. It was revealed that the photocatalytic performance of the synthesized nanocomposite was better than that for bare TiO₂ nanoparticles under sunlight irradiation. Furthermore, simple and fast magnetic recycling of the MNPs through the application of an external magnetic field was taken into account as the advantages. The results showed that the synthesized nanocomposite could be considered as an efficient photocatalyst in the field of wastewater treatment due to its lower band gap in the presence of γ -Fe₂O₃ nanoparticles.

Acknowledgements

The authors acknowledge the Bu-Ali Sina University Research Council and Center of Excellence in Development of Environmentally Friendly Methods for Chemical Synthesis (CEDEFMCS) for providing support to this work.

Notes

Corresponding author, Tel. / Fax: +98-811-8257407

E. mail: madrakian@basu.ac.ir, madrakian@gmail.com.

References

1. B. Palanisamy, C. M. Babu, B. Sundaravel, S. Anandan and V. Murugesan, *J. Hazard. Mater.*, 2013, **252–253**, 233.
2. W. Choi, *Catal. Surv. Asia*, 2006, **10**, 16.
3. M. R. Ghezzar, F. Abdelmalek, M. Belhadj, N. Benderdouche and A. Addou, *J. Hazard. Mater.*, 2009, **164**, 1266.
4. M. Addamo, M. Bellardita, D. Carriazo, A. Di Paola, S. Milioto, L. Palmisano and V. Rives, *Appl. Catal. B: Environ.*, 2008, **84**, 742.
5. F.-L. Toma, G. Bertrand, S. Begin, C. Meunier, O. Barres, D. Klein and C. Coddet, *Appl. Catal. B: Environ.*, 2006, **68**, 74.
6. M. F. S. Teixeira, M. F. Bergamini, C. M. P. Marques and N. Bocchi, *Talanta*, 2004, **63**, 108.
7. K. Nakata and A. Fujishima, *J. Photoch. Photobio. C*, 2012, **13**, 169.
8. B. Neppolian, H. C. Choi, S. Sakthivel, B. Arabindoo and V. Murugesan, *J. Hazard. Mater.*, 2002, **89**, 303.
9. M. Anpo and M. Takeuchi, *J. Catal.*, 2003, **216**, 505.
10. Y. Xia and L. Yin, *Phys. Chem. Chem. Phys.*, 2013, **15**, 18627.
11. T. Morikawa, T. Ohwaki, K.-i. Suzuki, S. Moribe and S. Tero-Kubota, *Appl. Catal. B: Environ.*, 2008, **83**, 56.
12. F. De Angelis, S. Fantacci, A. Selloni, M. K. Nazeeruddin and M. Grätzel, *J. Amer. Chem. Soc.*, 2007, **129**, 14156.

13. J. N. Clifford, E. Palomares, M. K. Nazeeruddin, M. Grätzel and J. R. Durrant, *J. Phys. Chem. C*, 2007, **111**, 6561.
14. A. Kay, I. Cesar and M. Grätzel, *J. Amer. Chem. Soc.*, 2006, **128**, 15714.
15. D. Mitoraj and H. Kisch, *Angew. Chem. Int. Ed.*, 2008, **47**, 9975.
16. G. Veréb, L. Manczinger, A. Oszkó, A. Sienkiewicz, L. Forró, K. Mogyorósi, A. Dombi and K. Hernádi, *Appl. Catal. B: Environ.*, 2013, **129**, 194.
17. K. Lv, B. Cheng, J. Yu and G. Liu, *Phys. Chem. Chem. Phys.*, 2012, **14**, 5349.
18. T. Hiroaki, M. Tomohiro, K. Tomokazu, A. Tomoki and T. Koji, *Nature Mater.*, 2006, **5**, 782.
19. M. Miyachi, A. Nakajima, K. Hashimoto and T. Watanabe, *Adv. Mater.*, 2000, **12**, 1923.
20. I. Nakamura, N. Negishi, S. Kutsuna, T. Ihara, S. Sugihara and K. Takeuchi, *J. Mol. Catal. A: Chem.*, 2000, **161**, 205.
21. I. Nakamura, S. Sugihara and K. Takeuchi, *Chem. Lett.*, 2000, **29**, 1276.
22. C. Wang, C. Shao, X. Zhang and Y. Liu, *Inorg. Chem.*, 2009, **48**, 7261.
23. J. Chen, L. Xu, W. Li and X. Gou, *Adv. Mater.*, 2005, **17**, 582.
24. B. Wang, J. S. Chen, H. B. Wu, Z. Wang and X. W. Lou, *J. Amer. Chem. Soc.*, 2011, **133**, 17146.
25. J. Zhu, Z. Yin, D. Yang, T. Sun, H. Yu, H. E. Hoster, H. H. Hng, H. Zhang and Q. Yan, *Energy Environ. Sci.*, 2013, **6**, 987.
26. P. Sun, Y. Liu, X. Li, Y. Sun, X. Liang, F. Liu and G. Lu, *RSC Adv.*, 2012, **2**, 9824.
27. T. Madrakian, A. Afkhami, M. Rahimi, M. Ahmadi and M. Soleimani, *Talanta*, 2013, **115**, 468.
28. A. Afkhami, R. Moosavi and T. Madrakian, *Talanta*, 2010, **82**, 785.
29. A. Afkhami, H. Bagheri and T. Madrakian, *Desalination*, 2011, **281**, 151.
30. W. Jiang, M. Pelaez, D. D. Dionysiou, M. H. Entezari, D. Tsoutsou and K. O'Shea, *Chem. Eng. J.*, 2013, **222**, 527.
31. A. Afkhami and R. Moosavi, *J. Hazard. Mater.*, 2010, **174**, 398.
32. A. H. A. Lee Kian Mun, Mohd Zobir Hussein, Zulkarnain Zainal, *Sains Malays.*, 2014, **43**, 437.
33. N. Sobti, A. Bensouici, F. Coloma, C. Untiedt and S. Achour, *J. Nanopart. Res.*, 2014, **16**, 1.
34. P. Mallick, *Mater. Sci-Pol*, 2014, **32**, 193.
35. A. D. Eaton, M. A. H. Franson, A. P. H. Association, A. W. W. Association and W. E. Federation, *Standard Methods for the Examination of Water & Wastewater*, American Public Health Association, 2005.
36. I. Langmuir, *J. Amer. Chem. Soc.*, 1916, **38**, 2221.
37. H. Freundlich and W. Heller, *J. Amer. Chem. Soc.*, 1939, **61**, 2228.
38. T. Madrakian, A. Afkhami, H. Mahmood-Kashani and M. Ahmadi, *J. Iran. Chem. Soc.*, 2013, **10**, 481.
39. Q. Wu, J. Ouyang, K. Xie, L. Sun, M. Wang and C. Lin, *J. Hazard. Mater.*, 2012, **199–200**, 410.
40. L. Peng, T. Xie, Y. Lu, H. Fan and D. Wang, *Phys. chem. chem. phys. : PCCP*, 2010, **12**, 8033.
41. M. I. Litter and J. A. Navío, *J. Photochem. Photobiol. A*, 1996, **98**, 171.
42. K. T. Ranjit and B. Viswanathan, *J. Photochem. Photobiol. A*, 1997, **108**, 79.